

This article appeared in a journal published by Elsevier. The attached copy is furnished to the author for internal non-commercial research and education use, including for instruction at the authors institution and sharing with colleagues.

Other uses, including reproduction and distribution, or selling or licensing copies, or posting to personal, institutional or third party websites are prohibited.

In most cases authors are permitted to post their version of the article (e.g. in Word or Tex form) to their personal website or institutional repository. Authors requiring further information regarding Elsevier's archiving and manuscript policies are encouraged to visit:

<http://www.elsevier.com/copyright>

JMBAvailable online at www.sciencedirect.com ScienceDirect

High-Resolution Orientation and Depth of Insertion of the Voltage-Sensing S4 Helix of a Potassium Channel in Lipid Bilayers

Tim Doherty[†], Yongchao Su[†] and Mei Hong^{*}

Department of Chemistry, Iowa State University, Ames, IA 50011, USA

Received 15 February 2010;
received in revised form
17 June 2010;
accepted 23 June 2010
Available online
30 June 2010

The opening and closing of voltage-gated potassium (Kv) channels are controlled by several conserved Arg residues in the S4 helix of the voltage-sensing domain. The interaction of these positively charged Arg residues with the lipid membrane has been of intense interest for understanding how membrane proteins fold to allow charged residues to insert into lipid bilayers against free-energy barriers. Using solid-state NMR, we have now determined the orientation and insertion depth of the S4 peptide of the KvAP channel in lipid bilayers. Two-dimensional ¹⁵N correlation experiments of macroscopically oriented S4 peptide in phospholipid bilayers revealed a tilt angle of 40° and two possible rotation angles differing by 180° around the helix axis. Remarkably, the tilt angle and one of the two rotation angles are identical to those of the S4 helix in the intact voltage-sensing domain, suggesting that interactions between the S4 segment and other helices of the voltage-sensing domain are not essential for the membrane topology of the S4 helix. ¹³C–³¹P distances between the S4 backbone and the lipid ³¹P indicate a ~9 Å local thinning and 2 Å average thinning of the DMPC (1,2-dimyristoyl-*sn*-glycero-3-phosphocholine)/DMPG (1,2-dimyristoyl-*sn*-glycero-3-phosphatidylglycerol) bilayer, consistent with neutron diffraction data. Moreover, a short distance of 4.6 Å from the guanidinium C^δ of the second Arg to ³¹P indicates the existence of guanidinium phosphate hydrogen bonding and salt bridges. These data suggest that the structure of the Kv gating helix is mainly determined by protein–lipid interactions instead of interhelical protein–protein interactions, and the S4 amino acid sequence encodes sufficient information for the membrane topology of this crucial gating helix.

© 2010 Elsevier Ltd. All rights reserved.

Edited by A. G. Palmer III

Keywords: membrane proteins; potassium channel voltage sensor; solid-state NMR; arginine-lipid interaction; helix orientation

Introduction

Voltage-activated potassium (Kv) channels are important for electrical signaling by neurons and muscle cells. The Kv voltage-sensing domain, which

contains four helices designated S1 to S4, drives the opening and closing of the potassium-conducting pore in response to changes in the membrane potential.^{1,2} Most of the gating charges are located on the S4 helix, which contains several conserved arginine residues (Arg) at every third position.³ High-resolution crystal structures^{4–6} and avidin accessibility measurements⁷ suggested that the S3b–S4 segment, which forms a helix–turn–helix motif called the voltage-sensing paddle, moves by as much as 15 Å during channel activation under depolarizing membrane voltages. Since positively charged Arg residues incur a high free-energy cost to insert into the low-dielectric hydrophobic core of lipid bilayers,⁸ there has been intense interest in understanding how the Arg-rich S4 helix is structured in the lipid bilayer in the resting and activated

^{*}Corresponding author. E-mail address: mhong@iastate.edu.

[†]T.H. and Y.S. contributed equally to this work.

Abbreviations used: Kv, voltage-activated potassium; TM, transmembrane; POPC, dioleoylphosphatidylcholine; POPG, dioleoylphosphatidylglycerol; CSA, chemical shift anisotropy; DMPC, 1,2-dimyristoyl-*sn*-glycero-3-phosphocholine; 6-O-PC, 1,2-di-*O*-hexyl-*sn*-glycero-3-phosphocholine; DMPG, 1,2-dimyristoyl-*sn*-glycero-3-phosphatidylglycerol; MAS, magic-angle spinning.

states of the protein. The paddle model proposes that the gating Arg residues interact directly with the lipids,⁵ while the canalculi model proposes that the Arg residues are shielded by acidic residues in other transmembrane (TM) helices.⁹ Molecular dynamics simulations of the S4 helix alone¹⁰ and of the entire voltage-sensing domain^{11,12} suggested that Arg-phosphate salt bridges, water clusters near the guanidinium moieties deep in the membrane, and membrane thinning contribute to the stabilization of the S4 Arg residues in the lipid membrane. Conductivity measurements showed that voltage sensing requires phosphate groups in lipid membranes,^{13,14} also supporting the notion that the voltage-sensing domain interacts strongly with the lipid headgroups. Neutron diffraction of the KvAP S1–S4 domain in POPC (dioleoyl phosphatidylcholine)/POPG (dioleoyl phosphatidylglycerol) bilayers showed that the voltage sensor is fully embedded in the lipid bilayer and does not cause strong perturbations of the membrane structure.¹⁵ Despite this increasing body of evidence, atomic-level structural information of the Kv voltage-sensing paddle and the Arg residues therein, measured directly in phospholipid bilayers, remains scarce.

Solid-state NMR spectroscopy has contributed significantly to the understanding of the structural basis for the function of Arg-rich membrane peptides such as antimicrobial peptides^{16,17} and cell-penetrating peptides.^{18,19} These studies demonstrated the feasibility of measuring interatomic distances between Arg residues and lipid phosphates in multilamellar lipid membranes. In addition, due to the intrinsic orientation dependence of NMR frequencies, solid-state NMR spectroscopy is a sensitive probe of the orientation of membrane proteins in lipid bilayers. Here, we combine static oriented-membrane solid-state NMR techniques with magic-angle spinning (MAS) experiments to determine the orientation, depth of insertion, and Arg-phosphate interaction of the Kv S4 peptide in

phospholipid bilayers. We compare these results with the structure of the S4 helix in the intact voltage sensor to infer the importance of lipid–protein *versus* protein–protein interactions for channel gating.

Results

S4 backbone conformation in the lipid bilayer

Before determining the S4 peptide orientation, we first measured the backbone conformation of the KvAP S4 peptide (residues 113–130) to confirm if this segment is α -helical in the lipid membrane in the absence of the other helices of the voltage-sensing domain. For this purpose, we measured the ^{13}C isotropic chemical shifts of six labeled residues distributed throughout the segment: Gly2, Leu6, Val7, Arg8, Leu9, and Ile15. A representative two-dimensional (2D) ^{13}C – ^{13}C DARR²⁰ correlation spectrum is shown in Fig. 1a. The difference of the C^α , C^β , and CO isotropic chemical shifts from the random-coil values gives information about the protein secondary structure.²¹ Figure 1b shows that most residues exhibit positive CO and C^α secondary shifts and negative C^β secondary shifts, which are characteristic of the α -helical conformation. The only exception is the N-terminal Gly2, which is consistent with the fact that the corresponding Gly114 in the intact KvAP voltage sensor is part of the turn between the S3b and S4 helices.⁴

S4 helix orientation in the lipid bilayer

The S4 helix orientation was determined using a 2D ^{15}N NMR experiment that correlates the ^{15}N – ^1H dipolar coupling with the ^{15}N chemical shift anisotropy (CSA) of uniaxially aligned peptides.²² Due to the periodic orientation distribution of the backbone N–H bonds with respect to the helix axis and the

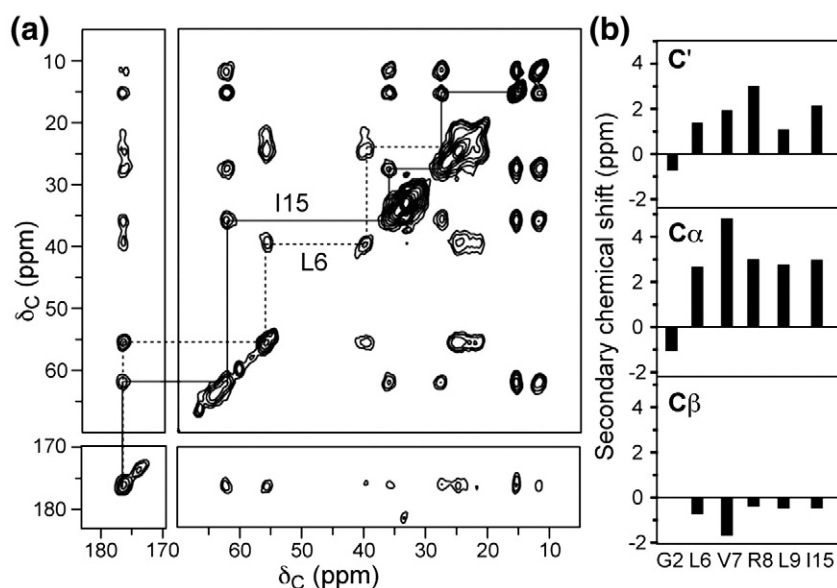


Fig. 1. ^{13}C isotropic chemical shifts of the KvAP S4 peptide in DMPC/DMPG bilayers. (a) 2D ^{13}C – ^{13}C correlation spectrum of Leu6, Ile15-labeled S4 at 263 K, with a spin diffusion mixing time of 30 ms. (b) Secondary chemical shifts of CO, C^α , and C^β of labeled residues, using random-coil chemical shifts of Ref. 21 (Table S1).

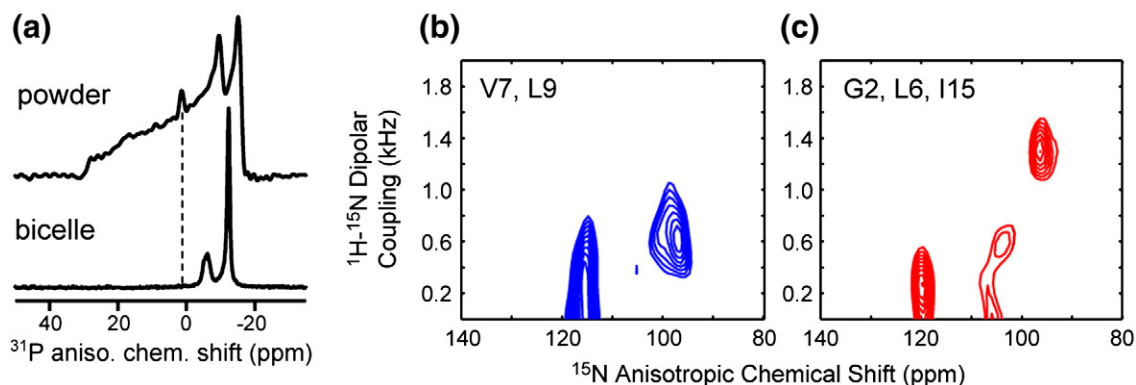


Fig. 2. Static orientation-dependent spectra of KvAP S4. (a) ^{31}P spectra of S4-containing unoriented DMPC/DMPG membranes (top) and magnetically aligned DMPC/6-O-PC bicelles (bottom). The minor peak at 0 ppm (top) is the phosphate buffer signal. (b and c) 2D N–H dipolar and ^{15}N CSA correlation spectra of bicelle aligned S4 peptide. (b) Val7, Leu9 ^{15}N -labeled S4 peptide. (c) Gly2, Leu6, and Ile15 ^{15}N -labeled S4 peptide.

relative orientation of the ^{15}N chemical shift tensor to the N–H bond, these 2D spectra exhibit wheel-like patterns^{23,24} whose position and size indicate the tilt angle of the helix from the bilayer normal. The position of individual resonances on these “PISA” wheels indicates the directions of the side chains around the helical axis.

We oriented the S4 peptide using magnetically aligned DMPC (1,2-dimyristoyl-*sn*-glycero-3-phosphocholine)/6-O-PC (1,2-di-*O*-hexyl-*sn*-glycero-3-phosphocholine) bicelles. Static ^{31}P spectra show sharp peaks at frequencies consistent with well-aligned bicelles whose bilayer normal is perpendicular to the magnetic field (Fig. 2a). No isotropic ^{31}P peak was observed in the bicelle spectrum, and the unoriented spectrum of S4-containing DMPC/DMPG (1,2-dimyristoyl-*sn*-glycero-3-phosphatidylglycerol) bilayers also shows a uniaxial powder pattern except for a phosphate buffer peak, indicating that the peptide does not perturb the bilayer integrity. The absence of strong membrane perturbation is consistent with neutron diffraction data of the S1–S4 domain in POPC/POPG membranes.¹⁵

Figure 2b and c shows the 2D ^{15}N correlation spectra of the oriented S4 peptide: the Val7, Leu9-labeled sample shows an N–H dipolar splitting of 1.2 kHz (read as twice the value from the zero-frequency axis) for one residue and nearly vanishing coupling for the other (Fig. 2b), while the triply Gly2, Leu6, Ile15-labeled sample shows a maximum N–H splitting of 2.8 kHz (Fig. 2c). The latter spectrum can be partially assigned on the basis of the ^{15}N -labeled positions: Leu6 and Ile15 should differ in their ρ angles by 180° , since every consecutive residue in an α -helix increments the ρ angle by 100° . Thus, Leu6 and Ile15 peaks should appear on opposite sides of the PISA wheel. As a result, the 120 ppm and 95 ppm peaks in Fig. 2c must be assigned to Leu6 and Ile15, while the weak signal at 106 ppm can be assigned to Gly2. Its nearly vanishing coupling is consistent with the unstructured nature of Gly2 obtained from the ^{13}C isotropic chemical shifts. Since Gly2 is not part of the α -helix, we do not consider its ^{15}N frequencies in the following orientation analysis.

Figure 3a compares the sum of the two experimental spectra with simulated 2D PISA wheel spectra for an ideal α -helix with tilt angles of 0° to 90° . The best-fit τ is found at 40° , where the position and size of the wheel are in excellent agreement with the experimental spectrum. The observed linewidths are 4–5 ppm for the ^{15}N anisotropic chemical shift dimension and 0.4–0.5 kHz for the dipolar dimension. These linewidths allow the tilt angle to be determined with a precision better than 5° , as shown in Fig. S1. A survey of published oriented membrane protein spectra shows that the ^{15}N anisotropic chemical shift linewidths range from 2.5 to 9 ppm, while the N–H dipolar coupling dimension has linewidths of 0.3–1.2 kHz. This linewidth variation reflects the intrinsic conformational distribution and dynamic disorder of the different membrane proteins.^{26–31}

To extract the ρ angle, we require that not only should the individual resonance positions on the $\tau=40^\circ$ wheel have minimal deviations from the measured frequencies, but also the order of peaks around the PISA wheel should follow the intrinsic orientation relationships of the N–H bonds. Excluding Gly2, the order of the four residues in the clockwise direction should be Leu6, Leu9, Ile15, and Val7. Figure 3b–d shows simulated spectra for several ρ angles, where the RMSD between the simulated and experimental spectra is indicated. The $\rho=0^\circ$ spectrum is an example of poor fit with large RMSD, while $\rho=100^\circ\pm 20^\circ$ and $280^\circ\pm 20^\circ$ show good agreement with the experimental spectra and correspond to the two RMSD minima in the full 360° range (Fig. S2). Moreover, the peak assignments are consistent with the known ^{15}N -labeled positions in the two samples. The difference of 180° in the two ρ solutions is not coincidental, since Leu6 and Ile15 differ in ρ by 180° , while Val7 and Leu9 differ in ρ by 200° ; thus, the two ρ angles are nearly degenerate. Although the RMSD values indicate that $\rho=280^\circ$ agrees better with the experimental spectra, due to the near-degeneracy we consider both orientations in the subsequent structural analysis that combines the insertion depth and the peptide orientation.

Depth of insertion of S4 residues and Arg–phosphate interaction

We probed the insertion depth of the S4 helix through ^{13}C – ^{31}P distances between the peptide and the lipid. C^α – P distances indicate the backbone immersion depths, while the Arg C^ζ distance to ^{31}P identifies possible salt bridges and snorkeling.³² The ^{31}P atoms lie in lamellar planes in our membrane samples based on the lack of isotropic peaks in the static ^{31}P spectra of both oriented bicelles and unoriented liposomes (Fig. 2). Figure 4 shows representative ^{13}C – ^{31}P REDOR data. Arg8 guanidinium C^ζ shows the shortest ^{13}C – ^{31}P distance of 5.5 Å when fit with a single distance. When the slower dephasing at long mixing times was taken into account, a 1:1 combination of a 4.6 and a 7.8 Å distance was found to best reproduce the data. Thus, at least 50% of the Arg8 guanidinium lies within hydrogen-bonding distance to the lipid phosphate headgroups.

Compared to Arg8, the hydrophobic residues all exhibit longer distances to ^{31}P . Leu6 and Ile15 C^α are 7.5 Å from the ^{31}P plane, while Val7 has an even longer C^α – P distance of 8.5 ± 1.0 Å. These distances were obtained using two-spin REDOR simulations. For fast REDOR dephasing such as that of Arg8 C^ζ , only one ^{31}P atom can approach the peptide ^{13}C closely due to the average 10 Å ^{31}P – ^{31}P separation in the membrane plane. For slower REDOR dephasing that corresponds to a nominal two-spin distance of 7 Å or longer, multiple ^{31}P atoms can interact with each ^{13}C spin. In this case, we have previously shown by multispin REDOR simulations¹⁶ that although the individual ^{13}C – ^{31}P distances are longer than the nominal value obtained from two-spin simulations, the vertical distance between the ^{13}C atom and the ^{31}P plane, which is the relevant parameter for reporting membrane protein depths, approaches the nominal two-spin distance. Thus,

the two-spin simulated distances here can be used to reflect the depth of the ^{13}C spins to the membrane plane.

Val7 and Ile15 C^α signals overlap with the lipid glycerol G3 and G1 carbon atoms, which have short distances to ^{31}P . Thus, in the REDOR simulation, we corrected for the lipid intensity contribution using the equation $(S/S_0)_{\text{observed}} = 0.76(S/S_0)_{\text{peptide}} + 0.12(S/S_0)_{\text{G1}} + 0.12(S/S_0)_{\text{G3}}$, where the coefficients were obtained from the lipid/peptide molar ratio. This natural-abundance correction was confirmed by a double-quantum filtered REDOR experiment¹⁹ on the Val7-labeled S4 peptide, which removed the lipid ^{13}C signals (Fig. S5). The resulting REDOR S/S_0 value supports the natural-abundance corrected REDOR distance of 8.5 Å (Fig. 4c).

Discussion

The ^{13}C isotropic chemical shifts indicate that most labeled residues in the S4 peptide exhibit the α -helical conformation in lipid bilayers,²¹ consistent with the conformation of this domain in the intact protein.^{4,6} The only nonhelical residue is the N-terminal Gly2, which is also consistent with the turn conformation of the corresponding Gly114 between S3b and S4 helices in the intact KvAP voltage sensor.

The 2D ^{15}N anisotropic correlation spectra indicate that the S4 helix deviates significantly from the limiting cases of a fully TM orientation ($\tau = 0^\circ$) or a fully in-plane orientation ($\tau = 90^\circ$). Spectral simulations yielded a tilt angle of $40 \pm 5^\circ$ and two ρ angles differing by 180° around the helix axis (Fig. 5). The data do not allow unambiguous determination of which ρ is adopted by the peptide, and it is possible that both are populated in the absence of other TM helices of the voltage sensor. Although not all residues of the peptide were ^{15}N -labeled, the inclusion of residues 6 and 15 among the labeled

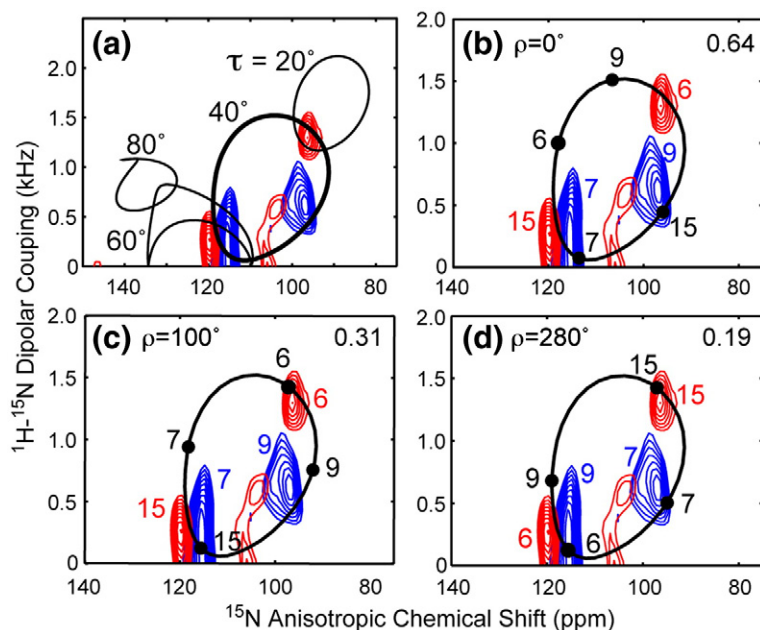


Fig. 3. Simulated orientation-dependent spectra of the KvAP S4 peptide. (a) Simulated 2D ^{15}N – ^1H dipolar and ^{15}N CSA correlation spectra (black lines) overlaid with the sum of the two experimental spectra of Fig. 2b and c. Best fit is $\tau = 40^\circ \pm 5^\circ$. Simulated spectra used a general order parameter of 0.8, estimated from Fig. S4.²⁵ (b–d) Simulated 2D spectra for $\tau = 40^\circ$ and different ρ angles. (b) $\rho = 0^\circ$. (c) $\rho = 100^\circ$. (d) $\rho = 280^\circ$. The assignment in the simulated spectra is annotated in black, while the assignment for the experimental spectrum is shown in color. The RMSD between the calculated and measured spectra is indicated in the upper right corner of each panel.

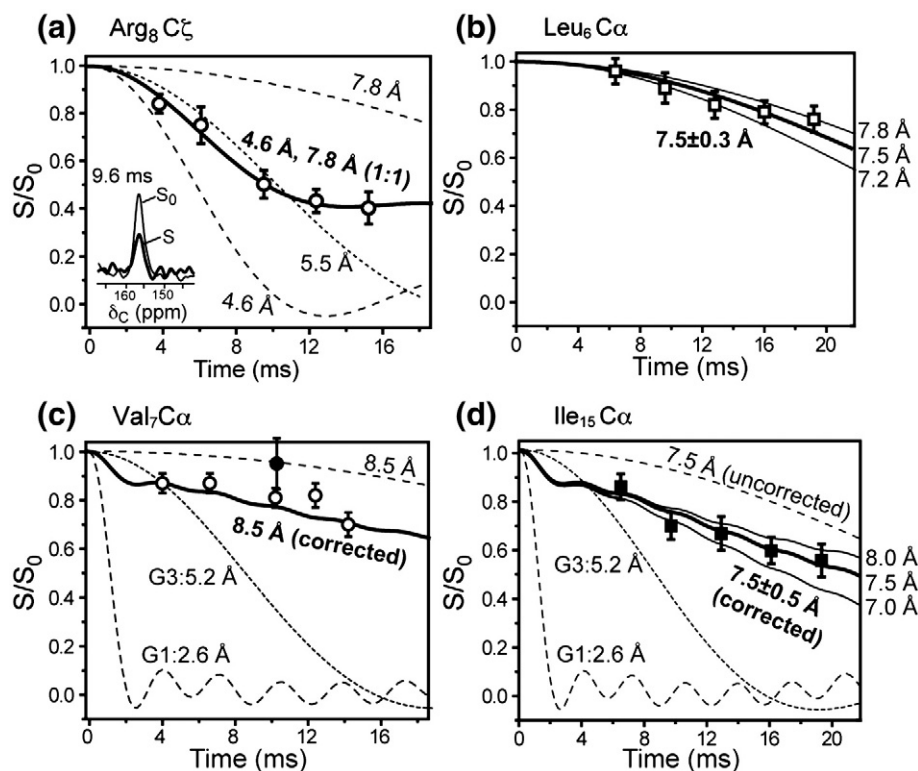


Fig. 4. Representative ^{13}C - ^{31}P REDOR data of the S4 peptide bound to DMPC/DMPG membranes. (a) Arg8 C^ζ data. Best fit involves a 1:1 combination of a short distance of 4.6 ± 0.2 Å and a long distance of 7.8 Å with an error bar of -0.6 and $+1.2$ Å (Fig. S6). The single-distance best fit is 5.5 Å. Representative control (S_0 , thin line) and dephased spectra (S , thick line) are shown in the inset. (b) Leu6 C^α , with a best-fit distance of 7.5 ± 0.3 Å. (c) Val7 C^α , with a best-fit distance of 8.5 ± 1.0 Å. (d) Ile15 C^α , with a best-fit distance of 7.5 ± 0.5 Å. For (c) and (d), the simulated REDOR decay curves (continuous lines) were corrected for lipid G1 and G3 intensities, whose distances to ^{31}P are fixed (dashed lines). In (c), a double-quantum REDOR data point (filled circle) falls on the uncorrected REDOR curve for 8.5 Å, confirming the single-quantum corrected REDOR distance simulation. All simulated REDOR curves are two-spin distances, which reflect the vertical distance of the ^{13}C - to the ^{31}P -containing membrane plane for distances within 7–9 Å.¹⁶

sites suggests that the tilt angle is valid for the central majority of the helix. Additional simulations show that the best-fit spectrum agrees with the experimental spectra to within $\pm 5^\circ$ for the tilt angle (Fig. S1). It has been shown that PISA wheels are sensitive not only to helix orientation but also to backbone (ϕ , ψ) angles.³³ Nonidealities greater than $\pm 4^\circ$ in the (ϕ , ψ) angles produce significant distortions in the PISA wheel pattern. For the orientation simulations, we used α -helical (ϕ , ψ) angles of (-64° , -40°), which are within the angular ranges predicted by TALOS for residues Val7 and Arg8 (Table S2). The good agreement between the best-fit and experimental spectra of the S4 peptide suggests that the conformation of the C-terminal half of the peptide, although only labeled at Ile15 in this study, does not differ significantly from the α -helical structure.

Interestingly, the crystal structure of the paddle-chimaera channel showed residues 297 to 306 to be a 3_{10} helix.⁶ However, detailed examination of the conformation of membrane proteins in available crystal and solid-state NMR structures by Page *et al.* suggests that the low dielectric and anhydrous environment of the lipid bilayer disfavors the formation of 3_{10} helices, since 3_{10} helices increase

the exposure of the partial negative charge of the carbonyl oxygen atoms to the lipid membrane compared to α -helices.³³ Moreover, due to their significantly different (ϕ , ψ) angles, 3_{10} helices have clearly different 2D ^{15}N spectral patterns than the PISA wheels for α -helices³⁴ (Fig. S1). Additional ^{15}N -labeling of the C-terminal residues will be useful for verifying the exact conformation of the C-terminal portion of the S4 peptide in the lipid bilayer.

To compare the NMR-determined orientation of the isolated S4 peptide with that in the intact voltage sensor, we show the 2.4 Å crystal structure of the voltage-sensing domain of the paddle-chimaera channel in Fig. 5c and d. The tetramer structure was taken from the Protein Data Bank (PDB; accession code 2R9R).⁶ The S4 helix and the S4–S5 linker helix were colored to guide the eye, and the pore helices S5 and S6 were removed from view for clarity. The crystal structure was solved using crystals grown in a mixture of detergents and phospholipids,⁶ where the S4 helix was that of the Kv2.1 potassium channel with a different amino acid sequence from the KvAP S4 sequence. However, the S3b–S4 voltage-sensor paddle has been shown to be transferable among voltage sensors of different

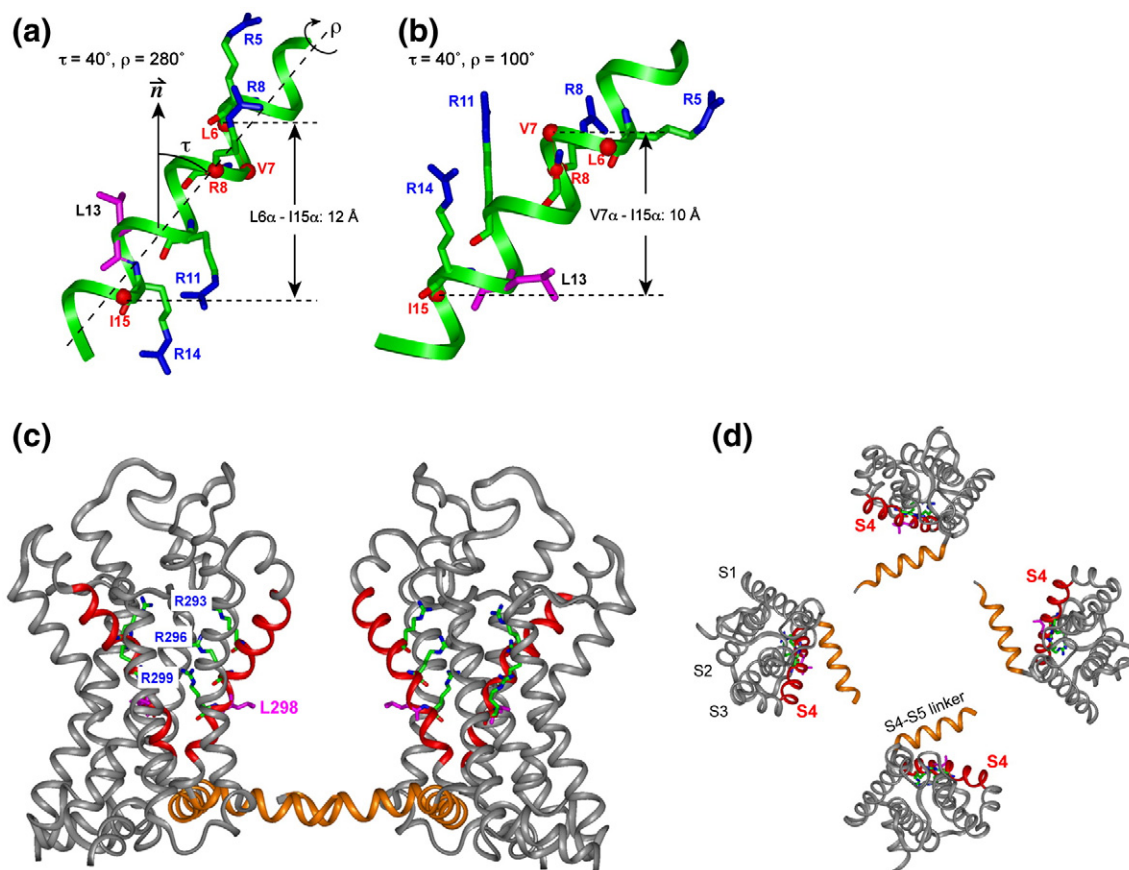


Fig. 5. Orientation of the S4 helix of Kv channels from NMR and crystal structures. (a and b) Solid-state NMR determined the orientation of the isolated S4 helix in lipid bilayers. (a) $\tau = 40^\circ$ and $\rho = 280^\circ$. (b) $\tau = 40^\circ$ and $\rho = 100^\circ$. The four Arg side chains and the Leu13 side chain are shown as sticks. C α atoms whose distances to lipid ^{31}P were measured are shown as balls. (c and d) X-ray crystal structure of the voltage-sensing domain of the Kv2.1–Kv1.2 paddle-chimaera channel.⁶ (c) Side view with the pore axis oriented vertically. (d) Top view of the tetramer. The S4 helix is highlighted in red, and the S4–S5 linker is in orange. The three Arg residues corresponding to the second to fourth Arg residues in the NMR samples, and Leu298 (pink), corresponding to Leu13 of the NMR samples, are shown as sticks.

origins,³⁵ and three of the four Arg residues are conserved between KvAP and Kv2.1; thus, the S4 helix is expected to be comparable between the crystal structure construct and the NMR sample studied here. We extracted the tilt angle of the S4 helix by comparing the average N–H bond orientation of each helix with the orientation of the 4-fold symmetry axis of the tetramer and found the tilt angle to be 43° for all four helices.

Within experimental uncertainty, the NMR-determined $40 \pm 5^\circ$ tilt angle of the isolated S4 peptide is identical to the 43° tilt of the S4 helix in the intact voltage sensor. Even more strikingly, Fig. 5 shows that one of the two NMR rotation angle solutions, $\rho = 100^\circ$, agrees very well with the side-chain directions of the S4 in the intact voltage sensor.⁶ Using the hydrophobic Leu13 between the third and fourth Arg (Arg11 and Arg14) as a point of reference, since the Leu rotameric state is relatively well defined,³⁶ we found that the Leu13 side chain in the isolated peptide has an orientation similar to that of the corresponding Leu298 in the intact voltage sensor. The remarkable similarities in τ and ρ angles indicate that the isolated S4 helix, bound to the lipid

bilayer, already adopts its final orientation in the intact S1–S4 domain. This in turn suggests that the S4 structure in the membrane is mainly dictated by the lipid–protein interaction and the S4 amino acid sequence and is only minimally affected by interactions with the other helices in the voltage sensor. In the crystal structure, the two C-terminal Arg residues of the S4 helix interact with glutamate residues in the S1 and S2 helices, while the two N-terminal Arg residues interact mainly with lipid phosphates and water.⁶ The preservation of the S4 orientation in the absence of the acidic residues suggests that the two lipid-interacting Arg residues may be largely sufficient for determining the global topology of the membrane-bound S4 helix.

Since the S4 peptide is mostly hydrophobic, the non-Arg residues are not expected to interact significantly with the polar lipid headgroups. If the Arg residues were not present, we suspect that the peptide orientation will be less tilted, like the WALP peptides,³⁷ to better match the thickness of the lipid bilayer. We speculate that the tendency of Arg residues to interact with the lipid phosphates and snorkel their side chains to the membrane surface

may be an important driving force for the observed tilted orientation of the S4 helix.

The short 4.6 Å distance between the C^ζ of the second Arg and the lipid ³¹P provides the first direct distance constraint for Arg–phosphate interactions in the Kv voltage sensor. Since the guanidinium C^ζ is surrounded by N–H groups, while the ³¹P is surrounded by oxygen atoms, the 4.6 Å C^ζ–P distance suggests N–H to O–P hydrogen bonding. This Arg–phosphate interaction is fully consistent with biochemical data that voltage gating is inhibited when the phosphate groups of lipids are enzymatically removed.^{13,14} In either orientation of Fig. 5a and b, all four Arg residues can adopt well-populated rotamers to bring their side chains toward the membrane surface ³¹P. For example, in the $\rho=280^\circ$ orientation, excellent Arg–headgroup contacts are established if Arg5, Arg8, Arg11, and Arg14 adopt the mtm85, ttp180, tpt85, and tpt85 rotamers, respectively, where t, p, and m represent 180°, +60°, and –60° (Fig. 5a). For $\rho=100^\circ$, guanidinium contacts with the membrane surfaces can be established if all four Arg residues adopt the mtt180 state, which is the second most populated Arg rotamer in α -helices³⁶ (Fig. 5b). Modeling shows that more than one rotameric state can allow guanidinium snorkeling to the bilayer surface. Indeed, the thermal disorder of the lipids and interactions with other helices of the voltage sensor may induce multiple rotamers for each Arg while still maintaining the salt bridge with the lipid phosphates.

The measured C^α–P distances confirm the implicit assumption (Fig. 5) that the S4 peptide is fully immersed in the lipid bilayer. Specifically, Ile15 has a similar C^α–P distance (7.5 Å) to Leu6 and Val7 C^α (7.5 and 8.5 Å), which are eight and nine residues apart. These distances rule out a half-inserted model (Fig. S3), since the vertical separation between Ile15 and Leu6 C^α or between Ile15 and Val7 C^α is too short compared to the combined C^α–P distances of ~16 Å: the separation is 8–10 Å for $\rho=100^\circ$ and 12–13 Å for $\rho=280^\circ$, which is 2–8 Å shorter than the sum of the C^α–P distances. Thus, the S4 peptide must be

fully inserted into the bilayer, in agreement with neutron diffraction data of the deuterated S1–S4 domain in POPC/POPG bilayers.¹⁵ For the fully inserted helix, combining the Val7–Ile15 C^α–C^α vertical distance of 10 Å, the Val7 C^α–P distance of 8.5 Å, and the Ile15 C^α–P distance of 7.5 Å, we obtain a P–P separation of 26 Å between the two membrane planes (Fig. 6a). This distance is 9 Å shorter than the unperturbed DMPC/DMPG bilayer thickness of 35 Å.³⁸ Thus, the distance and orientation data suggest that the DMPC/DMPG bilayer is thinned by about 9 Å at the site of S4 insertion. If residues Phe12 to Ile15 adopt the more extended ₃₁₀ conformation rather than the α -helical conformation, then the vertical separation between Val7 and Ile15 C^α would increase to about 13 Å, which would still indicate membrane thinning, but by about 6 Å.

Local thinning of phospholipid bilayers has been frequently observed before^{39–42} and is often associated with the function of membrane-active peptides.⁴³ Membrane thinning has also been seen in molecular dynamics simulations of the S4 helix.^{10,11} A thinning of 9 Å appears large at first. However, at the 1:5 peptide/lipid mass ratio used in the NMR samples, the 9 Å local thinning translates to a modest ~2 Å thinning averaged over the entire membrane, which is in excellent agreement with neutron diffraction data of the S1–S4 domain.¹⁵ This membrane thinning is almost certainly driven by the Arg–phosphate attraction, similar to what has been reported for Arg-rich antimicrobial peptides and cell-penetrating peptides.^{16,19} The membrane thinning would better allow the central two Arg residues, Arg8 and Arg11, to reach the membrane surfaces to establish guanidinium–phosphate contacts, further reducing the free energy of insertion.

How does the S4 amino acid sequence dictate the membrane-bound topology of the S4 helix? The helical wheel diagram (Fig. 6b) shows that the S4 peptide is actually quite hydrophobic despite the presence of four Arg residues and lacks a clear polar/nonpolar separation. The calculated hydrophobic moment (μ_H) of the peptide is only 2.0,⁴⁴ which is comparable to the μ_H of hydrophobic

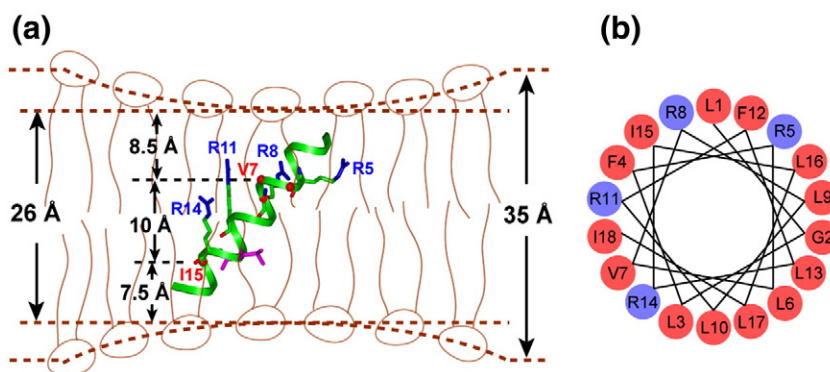


Fig. 6. Proposed membrane topology of the KvAP S4 peptide in lipid bilayers. (a) Orientation and depth of insertion of the peptide. S4 is fully inserted and causes a 9 Å thinning of the membrane at the site of peptide binding. (b) Helical wheel diagram of the S4 peptide, with hydrophobic residues in red and Arg residues in blue. The peptide has little amphiphilicity, supporting a TM motif.

membrane peptides such as the influenza A M2 TM domain.⁴⁵ In contrast, surface-bound membrane peptides such as magainin-2 and melittin have much higher μ_{H} values of 5–7. Thus, a TM topology of the S4 helix is actually not so surprising. Its significant tilt angle allows the four Arg residues to reach the membrane surface more readily than a helix that is completely parallel with the bilayer normal, since the latter backbone may cause steric conflicts with the Arg side chains.

The fact that the isolated S4 peptide adopts the same orientation as in the intact voltage-sensing domain suggests that S4 interactions with acidic residues in the rest of the voltage-sensing domain may not affect the global structural topology of this domain in the membrane, even though they may influence local structural features such as the side-chain conformations. Phospholipids and the intrinsic amino acid sequence appear to be sufficient for determining the membrane-bound orientation and depth of this important gating helix. The NMR data here thus support the model that the paddle directly interacts with the lipid bilayer during channel activation and deactivation. Perhaps it is not so surprising that the helix carrying the gating residues of the Kv channels has an intrinsic orientation that is not easily perturbed by the rest of the protein. The Kv voltage-sensing domain may have evolved to preserve the core structure and function of the S4 helix, making it dependent on the ubiquitous and less variable phospholipids of the cell membrane rather than the easily mutated protein residues.

Materials and Methods

Peptide and lipids

The segment corresponding to residues 113–130 of the voltage-sensing domain of KvAP, which is an archaeobacterial Kv channel from *Aeropyrum pernix*, was synthesized and purified using Fmoc chemistry (PrimmBiotech, Cambridge, MA). The amino acid sequence is LGLFRLVRL RFLRILLI. The corresponding amino acid sequence of the Kv2.1 segment in the paddle-chimaera crystal structure is VVQIFRIM RILIRFKL (residues 286–303),⁶ where the first two residues of the KvAP S4 peptide do not match any residues in the chimaera sequence. Except for the first Arg, the second to fourth Arg residues were conserved between the two sequences. Four KvAP S4 peptides were synthesized, incorporating a total of six ¹³C, ¹⁵N-labeled residues: Gly2, Leu6, Val7, Arg8, Leu9, and Ile15. The four samples were Gly2, Leu6, Ile15-labeled S4, Val7, Leu9-labeled S4, Val7, Arg8-labeled S4, and Leu6, Ile15-labeled S4.

DMPC, DMPG, and 6-O-PC were purchased from Avanti Polar Lipids.

Unoriented and oriented membrane samples

Unoriented hydrated proteoliposomes were prepared by mixing the peptide and lipids in organic solvents (3:1 chloroform/methanol) or in aqueous solution. A DMPC/DMPG (3:1) lipid mixture and a peptide/lipid molar ratio

of 1:16 were used for all unoriented samples for MAS experiments. For organic-solvent mixed samples, the peptide–lipid mixtures were lyophilized and rehydrated to 35 wt.% using a 10 mM (pH 7) phosphate buffer. For the aqueous-phase mixed samples, the peptide was dissolved in 2 mL of 30–60 mg/mL octyl- β -glucoside solution, mixed with the lipid vesicle solution at pH 7, then dialyzed against the buffer for 3 days to remove the detergent.⁴⁶ The proteoliposome solution was centrifuged at 150,000g at 6 °C to yield a homogeneous pellet. Excess water was removed by vacuum drying and the powder was then rehydrated to 35% water for MAS experiments.

Oriented DMPC/6-O-PC bicelles containing the peptide were prepared as described before.^{47–50} The lipid mixture was suspended in a 25 mM Hepes buffer (pH 7) to make a 35% (w/v) solution. The mixture was thermocycled between 0 and 42 °C three times and incubated at 4 °C overnight. The resulting homogenous solution was viscous at 42 °C but fluid at 0 °C, characteristic of bicelles. The degree of alignment of the bicelle in the magnetic field was examined by ³¹P NMR. KvAP S4 (2.5 mg) was mixed with 75 μ L of the bicelle solution, subjected to several thermocycles, and incubated at 4 °C until a homogenous solution was obtained.

Solid-state NMR experiments

MAS experiments were carried out on a Bruker DSX-400 (9.4 T) spectrometer at Larmor frequencies of 100.70 MHz for ¹³C and 162.1 MHz for ³¹P, using a triple-resonance 4-mm MAS probe. ¹³C and ³¹P chemical shifts were referenced to the α -glycine CO resonance at 176.49 ppm on the TMS scale and the hydroxyapatite ³¹P signal at 2.73 ppm on the phosphoric acid scale. Conformation-dependent ¹³C chemical shifts were measured using 2D ¹³C–¹³C DARR correlation experiments and a double-quantum (DQ) filtered experiment⁵¹ that removed the lipid ¹³C signals. The 2D experiments were conducted at 233–263 K under moderate spinning rates of 5.0 and 5.5 kHz. Low temperatures were achieved with a Kinetics Thermal Systems XR air-jet sample cooler (Stone Ridge, NY). Thermocouple-indicated temperatures were reported here. The actual sample temperature for both the moderate spinning MAS experiments and the static bicelle experiments is expected to be within 1–2 °C of the reported value.

A frequency-selective REDOR experiment^{52,53} was used to measure peptide–lipid ¹³C–³¹P distances. A selective ¹³C Gaussian pulse (0.8–1.0 ms) in the center of the REDOR period removed ¹³C–¹³C J couplings in the uniformly ¹³C-labeled residues, thus allowing ¹³C–³¹P REDOR effects to be observed at long mixing times. The experiments were carried out at 228 K, well below the phase transition temperature of the DMPC/DMPG membrane, to freeze lipid and peptide motions. Spinning speeds of 4.0 to 5.5 kHz were used for the REDOR experiments.

Static ³¹P and ¹⁵N NMR spectra for orientation determination were measured on a 600-MHz spectrometer (14.1 T). The static probe contained a solenoid coil whose axis is perpendicular to the magnetic field. ¹⁵N chemical shifts were externally referenced to the *N*-acetylvaline signal at 122 ppm on the NH₃ scale, and ³¹P chemical shifts were referenced to 85% H₃PO₄ at 0 ppm. The sample temperature was carefully chosen between 302 and 310 K to optimize bicelle alignment. For the 2D ¹H–¹⁵N dipolar chemical shift correlation (DIPSHIFT) experiment,²² the N–H evolution period followed the ¹H–¹⁵N cross-

polarization, and ^1H - ^1H homonuclear decoupling was achieved using the FSLG sequence,⁵⁴ whose scaling factor was directly measured to be 0.54 on model compounds. During ^{15}N detection, ^{13}C decoupling at 5 kHz removed the one-bond ^{15}N - ^{13}C dipolar coupling. This 2D experiment differs from the PISEMA experiment in the way the ^{15}N magnetization evolves during t_1 , but produces the same 2D spectral patterns as the PISEMA experiment.⁵⁵ Similar to PISEMA spectra, the static 2D DIPSHIFT spectra were plotted to show only half of the symmetric dipolar dimension, and simulated PISA wheels that cross over to the other half of the dipolar dimension were reflected back to the unique half.

Orientation calculation

Orientation-dependent 2D N-H/ ^{15}N correlation spectra were calculated for an ideal α -helix with $(\phi, \psi) = (-64^\circ, -40^\circ)$ as described before.²² Briefly, we defined a molecule-fixed frame whose z-axis was the helix axis, which was calculated as the average N-H vector orientation of 18 residues of the peptide. The y-z plane was defined as the common plane containing the helix axis and the CO-N vector between residues Leu3 and Phe4. The tilt angle τ was the angle between the helix axis and the bilayer normal, while the rotation angle ρ was the angle between the bilayer normal and the y-z plane of the molecular frame. $\rho = 0^\circ$ corresponds to the case when the bilayer normal lies in the y-z plane. In the Rose convention of Euler angles $\Omega(\alpha, \beta, \gamma)$, the rotation angle, which is uniquely determined by the protein sequence, corresponds to the azimuthal angle α ^{56,57} of the bilayer normal in the molecule-fixed frame. It differs from the azimuthal angle γ of the helix axis in a bilayer-fixed frame. The angle γ generally assumes all values, but for oriented samples whose alignment axis is parallel to the magnetic field, the NMR frequency is independent of γ . For oriented samples whose alignment axis is not coincident with the magnetic field, the different γ angles will lead to different anisotropic frequencies. However, bicelles undergo fast uniaxial rotation around the bicelle normal, thus averaging the γ angle and making the frequency dependent only on the tilt angle τ ($=\beta$) and the rotation angle ρ ($=\alpha$).

We simulated 2D spectra for τ between 0° and 90° in 5° steps and ρ between 0° and 360° in 20° steps. To obtain the best-fit orientation angles, we minimized the RMSD between the calculated and experimental 2D spectra using:²²

$$\text{RMSD} = \sqrt{\sum_i \left[\left(\frac{\omega_{\text{NH},i}^{\text{obs}} - \omega_{\text{NH},i}^{\text{sim}}}{\delta_{\text{NH}}^{\text{max}}} \right)^2 + \left(\frac{\omega_{\text{CSA},i}^{\text{obs}} - \omega_{\text{CSA},i}^{\text{sim}}}{\delta_{\text{CSA}}^{\text{max}}} \right)^2 \right]} \quad (1)$$

where the maximum N-H coupling $\delta_{\text{NH}}^{\text{max}}$ and ^{15}N CSA $\delta_{\text{CSA}}^{\text{max}}$ are:

$$\delta_{\text{NH}}^{\text{max}} = -\delta_{\text{NH}}^{\text{rigid}} \times 0.5 \times 0.8 \times 0.54 = 2.16 \text{ kHz} \quad (2)$$

$$\delta_{\text{CSA}}^{\text{max}} = -(\delta_{\text{zz}}^{\text{rigid}} - \delta_{\text{iso}}) \times 0.5 \times 0.8 + \delta_{\text{iso}} = 80 \text{ ppm} \quad (3)$$

In the above equations, we used a rigid-limit N-H coupling $\delta_{\text{NH}}^{\text{rigid}}$ of 10.0 kHz, ^{15}N z-principal value $\delta_{\text{NH}}^{\text{rigid}}$ of 227 ppm, and an ^{15}N isotropic shift δ_{iso} of 122 ppm. The factor of -0.5 is due to the 90° orientation of the bicelle axis from the magnetic field. The factor of 0.8 accounts for the

wobble of the bicelle axis, and was estimated from the ^{31}P CSA of the bicelles, which was 82–88% of the ^{31}P CSA of lipid bilayers (Table S3).^{25,48,58} This value was confirmed by simulations of the measured 2D ^{15}N spectra (Fig. S4). The scaling factor of 0.54 accounts for the homonuclear decoupling sequence of FSLG.

To visualize the peptide orientation, we affixed the best-fit bilayer normal to the molecule-fixed coordinate system defined above. The assembly of the peptide and the Cartesian system was then rotated such that the bilayer normal is vertical on the screen. The bilayer normal coordinates were inputted as $(x=r \sin \theta \cos \phi, y=r \sin \theta \sin \phi, z=r \cos \theta)$, where $\theta = \tau$ and $\phi = \rho + 90^\circ$.

To extract the orientation of the S4 helix in the crystal structure of the paddle-chimaera channel, we calculated the S4 helix axis as the average N-H bond orientation for 11 consecutive residues from 286 to 296. The choice of 11 residues was to complete three turns of the α -helix while not involving residues in the 3_{10} helix (from residue 297). Since the tetramer is symmetric, the channel axis orientation was the average orientation of the four S4 helix axes. The scalar product between the channel axis and each S4 helix axis gives the tilt angle.

Acknowledgements

T.D. is the grateful recipient of a Roy J. Carver Trust predoctoral training fellowship. This work is supported by NIH grant GM-066976.

Supplementary Data

Supplementary data associated with this article can be found, in the online version, at [doi:10.1016/j.jmb.2010.06.048](https://doi.org/10.1016/j.jmb.2010.06.048)

References

- Borjesson, S. I. & Elinder, F. (2008). Structure, function, and modification of the voltage sensor in voltage-gated ion channels. *Cell Biochem. Biophys.* **52**, 149–174.
- Swartz, K. J. (2008). Sensing voltage across lipid membranes. *Nature*, **456**, 891–897.
- Seoh, S. A., Sigg, D., Papazian, D. M. & Bezanilla, F. (1996). Voltage-sensing residues in the S2 and S4 segments of the Shaker K^+ channel. *Neuron*, **16**, 1159–1167.
- Jiang, Y., Lee, A., Chen, J., Ruta, V., Cadene, M., Chait, B. T. & MacKinnon, R. (2003). X-ray structure of a voltage dependent K^+ channel. *Nature*, **423**, 33–41.
- Jiang, Y., Ruta, V., Chen, J., Lee, A. & MacKinnon, R. (2003). The principle of gating charge movement in a voltage-dependent K^+ channel. *Nature*, **423**, 42–48.
- Long, S. B., Tao, X., Campbell, E. B. & MacKinnon, R. (2007). Atomic structure of a voltage-dependent K^+ channel in a lipid membrane-like environment. *Nature*, **450**, 376–383.
- Ruta, V., Chen, J. & MacKinnon, R. (2005). Calibrated measurement of gating-charge arginine displacement in the KvAP voltage-dependent K^+ channel. *Cell*, **123**, 463–475.

8. Hessa, T., Kim, H., Bihlmaier, K., Lundin, C., Boekel, J., Andersson, H. *et al.* (2005). Recognition of transmembrane helices by the endoplasmic reticulum translocon. *Nature*, **433**, 377–381.
9. Cuello, L. G., Cortes, D. M. & Perozo, E. (2004). Molecular architecture of the KvAP voltage-dependent K⁺ channel in a lipid bilayer. *Science*, **306**, 491–495.
10. Freites, J. A., Tobias, D. J., von Heijne, G. & White, S. H. (2005). Interface connections of a transmembrane voltage sensor. *Proc. Natl Acad. Sci. USA*, **102**, 15059–15064.
11. Sands, Z. A. & Sansom, M. S. P. (2007). How does a voltage sensor interact with a lipid bilayer? Simulations of a potassium channel domain. *Structure*, **15**, 235–244.
12. Jogini, V. & Roux, B. (2007). Dynamics of the Kv1.2 voltage-gated K⁺ channel in a membrane environment. *Biophys. J.* **93**, 3070–3082.
13. Schmidt, D., Jiang, Q. & MacKinnon, R. (2006). Phospholipids and the origin of cationic gating charges in voltage sensors. *Nature*, **444**, 775–779.
14. Xu, Y., Ramu, Y. & Lu, Z. (2008). Removal of phospho-head groups of membrane lipids immobilizes voltage sensors of K⁺ channels. *Nature*, **451**, 826–829.
15. Krepiy, D., Mihailescu, M., Freites, J. A., Schow, E. V., Worcester, D. L., Gawrisch, K. *et al.* (2009). Structure and hydration of membranes embedded with voltage-sensing domains. *Nature*, **462**, 473–479.
16. Tang, M., Waring, A. J. & Hong, M. (2007). Phosphate-mediated arginine insertion into lipid membranes and pore formation by a cationic membrane peptide from solid-state NMR. *J. Am. Chem. Soc.* **129**, 11438–11446.
17. Tang, M., Waring, A. J., Lehrer, R. I. & Hong, M. (2008). Effects of guanidinium-phosphate hydrogen bonding on the membrane-bound structure and activity of an arginine-rich membrane peptide from solid-state NMR. *Angew. Chem. Int. Ed. Engl.* **47**, 3202–3205.
18. Su, Y., Mani, R. & Hong, M. (2008). Asymmetric insertion of membrane proteins in lipid bilayers by solid-state NMR paramagnetic relaxation enhancement: a cell-penetrating peptide example. *J. Am. Chem. Soc.* **130**, 8856–8864.
19. Su, Y., Doherty, T., Waring, A. J., Ruchala, P. & Hong, M. (2009). Roles of arginine and lysine residues in the translocation of a cell-penetrating peptide from ¹³C, ³¹P, and ¹⁹F solid-state NMR. *Biochemistry*, **48**, 4587–4595.
20. Takegoshi, K., Nakamura, S. & Terao, T. (2001). ¹³C–¹H dipolar-assisted rotational resonance in magic-angle spinning NMR. *Chem. Phys. Lett.* **344**, 631–637.
21. Wang, Y. & Jardetzky, O. (2002). Probability-based protein secondary structure identification using combined NMR chemical-shift data. *Protein Sci.* **11**, 852–861.
22. Tang, M., Waring, A., Lehrer, R. & Hong, M. (2006). Orientation of a beta-hairpin antimicrobial peptide in lipid bilayers from two-dimensional dipolar chemical-shift correlation NMR. *Biophys. J.* **90**, 3616–3624.
23. Marassi, F. M. & Opella, S. J. (2000). A solid-state NMR index of helical membrane protein structure and topology. *J. Magn. Reson.* **144**, 150–155.
24. Wang, J., Denny, J., Tian, C., Kim, S., Mo, Y., Kovacs, F. *et al.* (2000). Imaging membrane protein helical wheels. *J. Magn. Reson.* **144**, 162–167.
25. Park, S., DeAngelis, A., Nevzorov, A., Wu, C. & Opella, S. (2006). Three-dimensional structure of the transmembrane domain of Vpu from HIV-1 in aligned phospholipid bicelles. *Biophys. J.* **91**, 3032–3042.
26. Hu, J., Asbury, T., Achuthan, S., Li, C., Bertram, R., Quine, J. R. *et al.* (2007). Backbone structure of the amantadine-blocked trans-membrane domain M2 proton channel from influenza A virus. *Biophys. J.* **92**, 4335–4343.
27. Li, C., Qin, H., Gao, F. P. & Cross, T. A. (2007). Solid-state NMR characterization of conformational plasticity within the transmembrane domain of the influenza A M2 proton channel. *Biochim. Biophys. Acta*, **1768**, 3162–3170.
28. Wang, J., Kim, S., Kovacs, F. & Cross, T. A. (2001). Structure of the transmembrane region of the M2 protein H⁺ channel. *Protein Sci.* **10**, 2241–2250.
29. Park, S. H., Mrse, A. A., Nevzorov, A. A., Mesleh, M. F., Oblatt-Montal, M., Montal, M. & Opella, S. J. (2003). Three-dimensional structure of the channel-forming trans-membrane domain of virus protein “u” (Vpu) from HIV-1. *J. Mol. Biol.* **333**, 409–424.
30. Thiriou, D. S., Nevzorov, A. A., Zagayanskiy, L., Wu, C. H. & Opella, S. J. (2004). Structure of the coat protein in Pf1 bacteriophage determined by solid-state NMR spectroscopy. *J. Mol. Biol.* **341**, 869–879.
31. Zeri, A. C., Mesleh, M. F., Nevzorov, A. A. & Opella, S. J. (2003). Structure of the coat protein in fd filamentous bacteriophage particles determined by solid-state NMR spectroscopy. *Proc. Natl Acad. Sci. USA*, **100**, 6458–6463.
32. Segrest, J. P., De Loof, H., Dohlman, J. G., Brouillette, C. G. & Anantharamaiah, G. M. (1990). Amphipathic helix motif: classes and properties. *Proteins*, **8**, 103–117.
33. Page, R. C., Kim, S. & Cross, T. A. (2008). Transmembrane helix uniformity examined by spectral mapping of torsion angles. *Structure*, **16**, 787–797.
34. Kim, S. & Cross, T. A. (2004). 2D solid-state NMR spectral simulation of ₃₁₀, α , and π -helices. *J. Magn. Reson.* **168**, 187–193.
35. Alabi, A. A., Bahamonde, M. I., Jung, H. J., Kim, J. I. & Swartz, K. J. (2007). Portability of paddle motif function and pharmacology in voltage sensors. *Nature*, **450**, 370–375.
36. Lovell, S. C., Word, J. M., Richardson, J. S. & Richardson, D. C. (2000). The penultimate rotamer library. *Proteins: Struct. Funct. Genet.* **40**, 389–408.
37. Strandberg, E., Morein, S., Rijkers, D. T. S., Liskamp, R. M. J., vanderWel, P. C. A. & Killian, J. A. (2002). Lipid dependence of membrane anchoring properties and snorkeling behavior of aromatic and charged residues in transmembrane peptides. *Biochemistry*, **41**, 7190–7198.
38. Kucerka, N., Liu, Y., Chu, N., Petrache, H. I., Tristram-Nagle, S. & Nagle, J. F. (2005). Structure of fully hydrated fluid phase DMPC and DLPC lipid bilayers using X-ray scattering from oriented multilamellar arrays and from unilamellar vesicles. *Biophys. J.* **88**, 2626–2637.
39. Heller, W. T., Waring, A. J., Lehrer, R. I., Harroun, T. A., Weiss, T. M., Yang, L. & Huang, H. W. (2000). Membrane-thinning effect of the β -sheet antimicrobial protegrin. *Biochemistry*, **39**, 139–145.
40. Yamaguchi, S., Huster, D., Waring, A., Lehrer, R. I., Tack, B. F., Kearney, W. & Hong, M. (2001). Orientation and dynamics of an antimicrobial peptide in the lipid bilayer by solid-state NMR. *Biophys. J.* **81**, 2203–2214.

41. Buffy, J., Hong, T., Yamaguchi, S., Waring, A., Lehrer, R. & Hong, M. (2003). Solid-state NMR investigation of the depth of insertion of protegrin-1 in lipid bilayers using paramagnetic Mn^{2+} . *Biophys. J.* **85**, 2363–2373.
42. Mecke, A., Lee, D. K., Ramamoorthy, A., Orr, B. G. & Banaszak Holl, M. M. (2005). Membrane thinning due to antimicrobial peptide binding: an atomic force microscopy study of MSI-78 in lipid bilayers. *Biophys. J.* **89**, 4043–4050.
43. Huang, H. W. (2006). Molecular mechanism of antimicrobial peptides: the origin of cooperativity. *Biochim. Biophys. Acta*, **1758**, 1292–1302.
44. Jaysinghe, S., Hristova, K., Wimley, W., Snider, C. & White, S. H. (2008). <http://blanco.biomol.uci.edu/mpex>.
45. Cady, S. D., Luo, W. B., Hu, F. & Hong, M. (2009). Structure and function of the influenza M2 proton channel. *Biochemistry*, **48**, 7356–7364.
46. Luo, W., Mani, R. & Hong, M. (2007). Side-chain conformation of the M2 transmembrane peptide proton channel of influenza A virus from 19F solid-State NMR. *J. Phys. Chem. B*, **111**, 10825–10832.
47. DeAngelis, A. & Opella, S. (2007). Bicelle samples for solid-state NMR of membrane proteins. *Nat. Protoc.* **2**, 2332–2338.
48. Marcotte, I. & Auger, M. (2005). Bicelles as model membranes for solid-state and solution-state NMR studies of membrane peptides and proteins. *Concept. Magn. Reson. A*, **24**, 17–37.
49. Prosser, R. S., Evanics, F., Kitevski, J. L. & Al-Abdul-Wahid, M. S. (2006). Current applications of bicelles in NMR studies of membrane-associated amphiphiles and proteins. *Biochemistry*, **45**, 8453–8465.
50. Aussenac, F., Lavigne, B. & Dufourc, E. (2005). Toward bicelle stability with ether-linked phospholipids: temperature, composition, and hydration diagrams by 2H and ^{31}P solid-state NMR. *Langmuir*, **21**, 7129–7135.
51. Hohwy, M., Jakobsen, H. J., Eden, M., Levitt, M. H. & Nielsen, N. C. (1998). Broadband dipolar recoupling in the nuclear magnetic resonance of rotating solids: a compensated C7 pulse sequence. *J. Chem. Phys.* **108**, 2686–2694.
52. Gullion, T. & Schaefer, J. (1989). Rotational echo double resonance NMR. *J. Magn. Reson.* **81**, 196–200.
53. Jaroniec, C. M., Tounge, B. A., Rienstra, C. M., Herzfeld, J. & Griffin, R. G. (1999). Measurement of ^{13}C - ^{15}N distances in uniformly ^{13}C labeled biomolecules: J-decoupled REDOR. *J. Am. Chem. Soc.* **121**, 10237–10238.
54. Bielecki, A., Kolbert, A. C., de Groot, H. J. M., Griffin, R. G. & Levitt, M. H. (1990). Frequency-switched Lee-Goldberg sequences in solids. *Adv. Magn. Reson.* **14**, 111–124.
55. Wu, C. H., Ramamoorthy, A. & Opella, S. J. (1994). High-resolution heteronuclear dipolar solid-state NMR spectroscopy. *J. Magn. Reson.* **109**, 270–272.
56. Schmidt-Rohr, K. & Spiess, H. W. (1994). *Multidimensional Solid-State NMR and Polymers*, 1st edit, Academic Press, San Diego.
57. Rose, M. E. (1957). *Elementary Theory of Angular Momentum*. Wiley, New York.
58. DeAngelis, A., Howell, S., Nevzorov, A. & Opella, S. (2006). Structure determination of a membrane protein with two trans-membrane helices in aligned phospholipid bicelles by solid-state NMR spectroscopy. *J. Am. Chem. Soc.* **128**, 12256–12267.